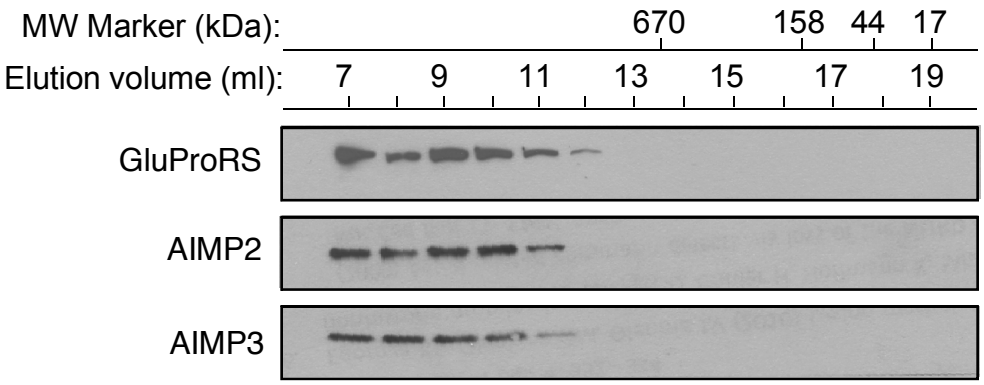


**Figure S1.** GluProRS in the MSC. HEK293T cells were grown in DMEM until 80-90% confluent. The cells were lysed in buffer containing 20 mM Tris-HCl (pH 7.5), 150 mM NaCl, 0.5% Triton X-100 and Protease Inhibitor Cocktail, and the debris cleared by ultracentrifugation at 100,000 g for 1 h. The cleared lysate (3 mg protein) was applied to a Superose-6 FPLC column, and eluted at a flow rate of 0.5 ml/min in buffer containing 50 mM Tris-HCl (pH 7.5), 150 mM NaCl, 1 mM phenylmethanesulfonyl fluoride, and 1 mM dithiothreitol. Thyroglobulin (6701 kDa), gamma globulin (158 kDa), ovalbumin (44 kDa), bovine serum albumin (66 kDa), myoglobin (17 kDa), and vitamin $B_{12}$ (1.35 kDa, not shown) served as molecular weight standards. Aliquots from alternate fractions were run on 4-20% SDS-PAGE for western blot analysis.

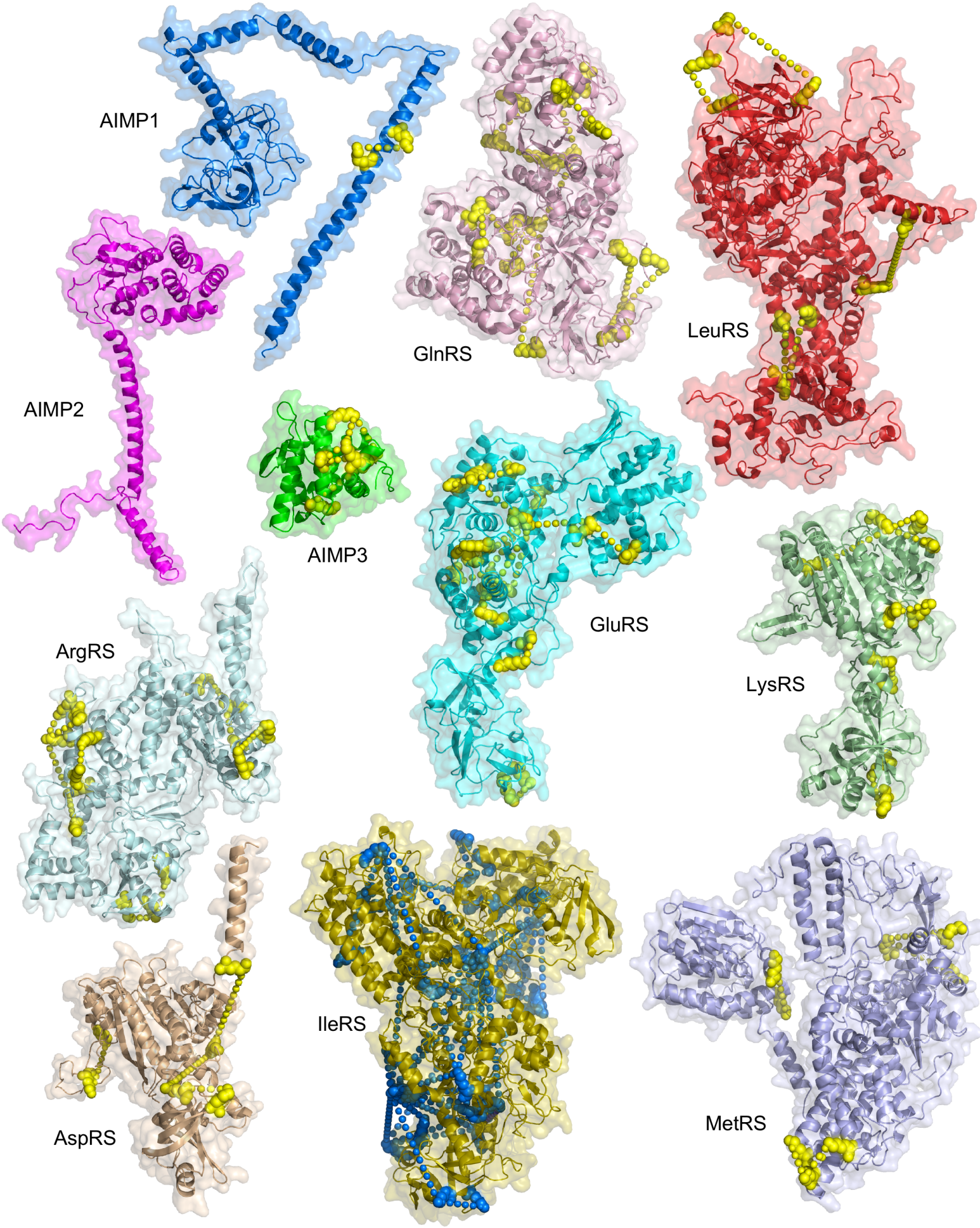


**Figure S2.** MSC constituent structures. X-ray structures after adjustment for intra- and inter-protein XL-MS crosslinks. Lys residues and their intra-protein cross-links shown as yellow spheres (or blue for IleRS).

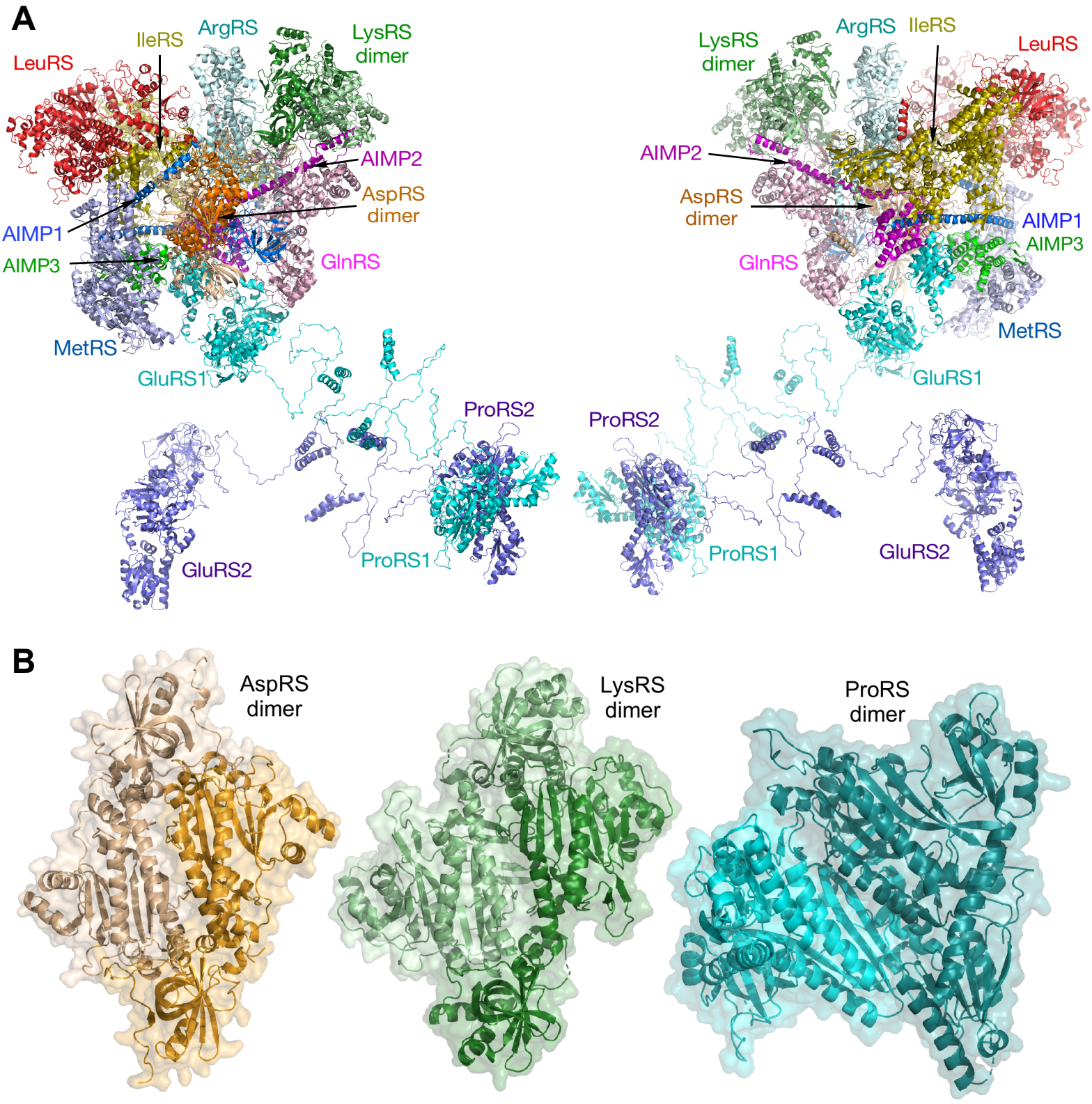


**Figure S3.** MSC structures with dimer constituents. (**A**) Ribbon models of front (left) and rear (right) views of the MSC including dimers of AspRS, LysRS, and GluProRS. (**B**) X-ray structures of AspRS (left, PDB ID: 4J15), LysRS (center, PDB ID: 6ILD), and ProRS (right, PDB ID: 4HVC) dimers.

**Supplementary Table S1.** Inter-protein cross-links identified by XL-MS.

| Peptide A | Peptide B | Occurrences, in-cell experiment (n=1) | Occurrences, on-bead experiments (n=3) |
|---|---|---|---|
| AIMP1 $K_{129}$ | ArgRS $K_{471}$ | - | 1 |
| | | | |
| AIMP2 $K_{64}$ | GlnRS $K_{759}$ | - | 2 |
| | | | |
| AIMP2 $K_{7}$ | LysRS $K_{249}$ | - | 3 |
| AIMP2 $Y_{35}$ | LysRS $K_{249}$ | - | 1 |
| AIMP2 $K_{64}$ | LysRS $K_{249}$ | - | 1 |
| | | | |
| AIMP3 $K_{138}$ | AspRS $K_{374}$ | 1 | 3 |
| | | | |
| ArgRS $K_{20}$ | GlnRS $K_{759}$ | - | 1 |
| ArgRS $K_{557}$ | GlnRS $K_{25}$ | - | 1 |
| | | | |
| ArgRS $K_{60}$ | IleRS $K_{382}$ | - | 1 |
| ArgRS $K_{522}$ | IleRS $K_{885}$ | 1 | - |
| | | | |
| ArgRS $K_{471}$ | LeuRS $K_{1102}$ | 1 | 1 |
| | | | |
| AspRS $K_{13}$ | GlnRS $K_{309}$ | - | 1 |
| | | | |
| AspRS $K_{451}$ | MetRS $K_{729}$ | - | 2 |
| | | | |
| GlnRS $K_{405}$ | GluProRS $K_{243}$ | 1 | - |
| GlnRS $K_{405}$ | GluProRS $K_{300}$ | 1 | 2 |
| GlnRS $K_{405}$ | GluProRS $K_{435}$ | 1 | - |
| | | | |
| IleRS $K_{382}$ | LeuRS $K_{1133}$ | - | 1 |
| IleRS $K_{450}$ | LeuRS $K_{1133}$ | 1 | 1 |
| | | | |
| IleRS $K_{996}$ | MetRS $K_{729}$ | - | 1 |

**Supplementary Table S2.** Intra-protein cross-links identified by XL-MS.

| Peptide A | Peptide B | Occurrences, in-cell experiment (n=1) | Occurrences, on-bead experiments (n=3) |
|---|---|---|---|
| | | | |
| AIMP1 | | | |
| $K_{54}$ | $K_{46}$ | - | 1 |
| | | | |
| AIMP3 | | | |
| $K_{88}$ | $K_{136}$ | - | 1 |
| $K_{88}$ | $K_{138}$ | 1 | 2 |
| $K_{96}$ | $K_{136}$ | - | 1 |
| $K_{96}$ | $K_{138}$ | - | 1 |
| $K_{105}$ | $K_{136}$ | - | 1 |
| | | | |
| ArgRS | | | |
| $K_{60}$ | $K_{68}$ | 1 | 1 |
| $K_{60}$ | $K_{557}$ | 1 | 2 |
| $K_{131}$ | $K_{143}$ | - | 1 |
| $K_{205}$ | $K_{321}$ | - | 1 |
| $K_{321}$ | $K_{471}$ | 1 | 3 |
| $K_{347}$ | $K_{362}$ | - | 1 |
| $K_{347}$ | $K_{393}$ | 1 | 2 |
| $K_{449}$ | $K_{522}$ | - | 1 |
| $K_{471}$ | $K_{476}$ | 1 | 1 |
| $K_{471}$ | $K_{478}$ | 1 | 3 |
| | | | |
| AspRS | | | |
| $K_{26}$ | $K_{40}$ | 1 | 3 |
| $K_{40}$ | $K_{55}$ | 1 | - |
| $K_{55}$ | $K_{122}$ | 1 | 1 |
| $K_{241}$ | $K_{451}$ | - | 1 |
| | | | |
| GlnRS | | | |
| $K_{19}$ | $K_{50}$ | - | 1 |
| $K_{25}$ | $K_{205}$ | 1 | 2 |
| $K_{25}$ | $K_{498}$ | 1 | 2 |
| $K_{25}$ | $K_{586}$ | 1 | 3 |
| $K_{25}$ | $K_{759}$ | - | 2 |
| $K_{50}$ | $K_{163}$ | - | 1 |
| $K_{233}$ | $K_{254}$ | - | 1 |
| $K_{309}$ | $K_{421}$ | - | 1 |
| $K_{309}$ | $K_{496}$ | - | 1 |
| $K_{366}$ | $K_{412}$ | 1 | 3 |
| $K_{366}$ | $K_{421}$ | - | 3 |
| $K_{366}$ | $K_{498}$ | 1 | 3 |
| $K_{628}$ | $K_{673}$ | 1 | 3 |
| $K_{628}$ | $K_{769}$ | 1 | 1 |
| $K_{628}$ | $K_{774}$ | - | 2 |
| | | | |
| GluProRS | | | |
| $K_{148}$ | $K_{173}$ | - | 1 |
| $K_{173}$ | $K_{417}$ | - | 2 |
| $K_{197}$ | $K_{231}$ | - | 1 |
| $K_{243}$ | $K_{300}$ | - | 1 |
| $K_{245}$ | $K_{435}$ | 1 | 3 |
| $K_{278}$ | $K_{282}$ | - | 1 |
| $K_{282}$ | $K_{288}$ | - | 1 |
| $K_{282}$ | $K_{417}$ | - | 1 |
| $K_{300}$ | $K_{435}$ | 1 | 2 |

| | | | |
|---|---|---|---|
| $K_{300}$ | $K_{437}$ | - | 1 |
| $K_{417}$ | $K_{472}$ | 1 | 3 |
| $K_{435}$ | $K_{437}$ | - | 2 |
| $K_{435}$ | $K_{472}$ | 1 | 3 |
| $K_{491}$ | $K_{498}$ | 1 | 3 |
| $K_{578}$ | $K_{593}$ | - | 1 |
| $K_{917}$ | $K_{922}$ | - | 1 |
| $K_{1010}$ | $K_{1034}$ | - | 1 |
| $K_{1089}$ | $K_{1109}$ | - | 1 |
| $K_{1091}$ | $K_{1109}$ | 1 | 3 |
| $K_{1109}$ | $K_{1156}$ | 1 | 3 |
| $K_{1143}$ | $K_{1156}$ | - | 1 |
| $K_{1156}$ | $K_{1213}$ | - | 2 |
| | | | |
| IleRS | | | |
| $K_{65}$ | $K_{132}$ | - | 2 |
| $K_{132}$ | $K_{149}$ | - | 1 |
| $K_{132}$ | $K_{169}$ | - | 2 |
| $K_{132}$ | $K_{382}$ | 1 | 2 |
| $K_{132}$ | $K_{410}$ | - | 2 |
| $K_{132}$ | $K_{450}$ | 1 | 3 |
| $K_{132}$ | $K_{641}$ | 1 | - |
| $K_{132}$ | $K_{672}$ | - | 1 |
| $K_{132}$ | $K_{996}$ | - | 2 |
| $K_{169}$ | $K_{450}$ | - | 1 |
| $K_{169}$ | $K_{672}$ | - | 1 |
| $K_{177}$ | $K_{450}$ | - | 1 |
| $K_{268}$ | $K_{382}$ | 1 | 3 |
| $K_{268}$ | $K_{410}$ | - | 2 |
| $K_{268}$ | $K_{450}$ | 1 | 1 |
| $K_{268}$ | $K_{996}$ | - | 1 |
| $K_{285}$ | $K_{288}$ | 1 | 3 |
| $K_{285}$ | $K_{450}$ | 1 | 3 |
| $K_{314}$ | $K_{450}$ | - | 1 |
| $K_{375}$ | $K_{382}$ | - | 3 |
| $K_{375}$ | $K_{450}$ | - | 1 |
| $K_{382}$ | $K_{410}$ | 1 | 3 |
| $K_{382}$ | $K_{450}$ | 1 | 2 |
| $K_{382}$ | $K_{996}$ | - | 1 |
| $K_{410}$ | $K_{450}$ | - | 1 |
| $K_{443}$ | $K_{450}$ | - | 1 |
| $K_{450}$ | $K_{641}$ | - | 3 |
| $K_{450}$ | $K_{996}$ | - | 1 |
| $K_{641}$ | $K_{672}$ | 1 | 2 |
| $K_{641}$ | $K_{903}$ | 1 | 2 |
| $K_{672}$ | $K_{725}$ | - | 1 |
| $K_{725}$ | $K_{816}$ | 1 | 3 |
| $K_{817}$ | $K_{861}$ | - | 1 |
| $K_{839}$ | $K_{1061}$ | 1 | - |
| $K_{861}$ | $K_{868}$ | - | 1 |
| $K_{868}$ | $K_{996}$ | 1 | 1 |
| $K_{878}$ | $K_{885}$ | - | 1 |
| $K_{878}$ | $K_{887}$ | 1 | 2 |
| $K_{885}$ | $K_{929}$ | - | 1 |
| $K_{887}$ | $K_{996}$ | - | 1 |
| $K_{903}$ | $K_{906}$ | 1 | 3 |
| $K_{996}$ | $K_{1061}$ | 1 | 3 |
| $K_{1014}$ | $K_{1057}$ | - | 1 |
| $K_{1016}$ | $K_{1057}$ | - | 1 |
| $K_{1051}$ | $K_{1104}$ | - | 1 |
| | | | |
| LeuRS | | | |

| | | | |
|---|---|---|---|
| $K_{270}$ | $K_{283}$ | - | 2 |
| $K_{278}$ | $K_{312}$ | - | 1 |
| $K_{807}$ | $K_{1002}$ | 1 | 3 |
| $K_{822}$ | $K_{1002}$ | 1 | 3 |
| $K_{1114}$ | $K_{1138}$ | - | 1 |
| | | | |
| LysRS | | | |
| $K_{135}$ | $K_{141}$ | 1 | 1 |
| $K_{223}$ | $K_{243}$ | - | 2 |
| $K_{305}$ | $K_{479}$ | 1 | 1 |
| $K_{363}$ | $K_{370}$ | - | 1 |
| $K_{402}$ | $K_{479}$ | 1 | 2 |
| $K_{407}$ | $K_{479}$ | 1 | 3 |
| | | | |
| MetRS | | | |
| $K_{108}$ | $K_{204}$ | - | 1 |
| $K_{375}$ | $K_{491}$ | 1 | 3 |
| $K_{491}$ | $K_{500}$ | - | 1 |
| $K_{663}$ | $K_{729}$ | 1 | 3 |
| $K_{726}$ | $K_{729}$ | 1 | 3 |

## Supplemental Data

# 3-Dimensional architecture of the human multi-tRNA synthetase Complex

**Modeling of individual MSC constituents**

*ArgRS.* A model of near full-length human ArgRS ($Asp_2$-$Met_{660}$) was built from the crystal structure of human ArgRS (chain B, PDB ID: 4R3Z (1)). The N-terminus domain ($Asp_2$-$Pro_{69}$) of ArgRS was relocated to satisfy Lys-Lys intra-molecular cross-links.

*AspRS.* A model of near full-length human AspRS monomer ($Ala_4$-$Asp_{495}$) was built from the crystal structure of human AspRS ($Ala_{21}$-$Asp_{495}$, PDB ID: 4J15 (2)) and a peptide ($Ala_4$-$Ala_{20}$) for the N-terminus modeled using SWISS-MODEL. Domains missing from this crystal structure, i.e., $Met_1$-$Ala_{20}$, $Glu_{163}$-$Ala_{172}$, $Ile_{224}$-$Ala_{247}$, $Arg_{273}$-$His_{282}$, and $Pro_{496}$-$Pro_{501}$ were constructed in the model except for $Pro_{496}$-$Pro_{501}$. To generate the cross-link between the N-terminus of AspRS ($Lys_{13}$) and GlnRS ($Lys_{309}$) a *de novo*-built $\alpha$-helical peptide ($Ala_4$-$Ala_{20}$) was appended and the conformation of $Ala_{21}$-$Asp_{50}$ domain adjusted to satisfy the AspRS-GlnRS intermolecular crosslink. For construction of the MSC model with the AspRS dimer, the second chain was added by aligning chain A from the crystal structure of AspRS (PDB ID: 4J15 (2)) with the monomer in the MSC model. Maintaining the observed crosslinks between ArgRS and GlnRS induced some overlap of AspRS chain B with ArgRS.

*GlnRS.* A model of full-length human GlnRS ($Met_1$-$Val_{775}$) was built starting from the crystal structure of human GlnRS ($Met_1$-$Asp_{771}$) (PDB ID: 4YE6 (3)). Domains missing from this crystal structure, i.e., $Ala_{183}$-$Gln_{216}$, $Glu_{363}$-$Asn_{369}$, $Glu_{459}$-$Gln_{461}$, $Ala_{585}$-$Leu_{588}$, $Leu_{630}$-$Leu_{638}$, $Ala_{668}$-$Lys_{673}$, and $Pro_{772}$-$Val_{775}$, were constructed with SWISS-MODEL. The N-terminus domain ($Met_1$-$Glu_{182}$) was relocated with respect to the catalytic domain to satisfy XL-MS-derived intra-molecular crosslinks.

*GluRS.* A model of near full-length ($Ala_2$-$Gln_{682}$) human GluRS was assembled from the crystal structures of the GST-like domain ($Ala_2$-$Thr_{171}$) of human GluRS (chain C, PDB ID: 5Y6L (4)) and the catalytic domain ($Leu_{87}$-$Lys_{533}$) of GluRS from archaeal

*Methanothermobacter thermautotrophicus* (PDB ID: 3AII (5)) corresponding to $Phe_{187}$-$Gln_{682}$ in human GluRS, plus a *de novo*-built spacer ($Thr_{172}$-$Lys_{186}$) joining the GluRS GST-like and CD domains to satisfy intra-molecular cross-links.

*GluProRS.* A three-dimensional model of A and B chains of full-length human GluProRS ($Ala_2$-$Tyr_{1512}$) was assembled from human GluRS monomer, a model of the WHEP domain-containing linker ($Pro_{683}$-$Gly_{1015}$), and the crystal structure of ProRS dimer (PDB ID: 4HVC, (6)). The crystal structure of the multifunctional peptide motif-1 (helix-turn-helix, WHEP domain 1) from human GluProRS (PDB ID: 1FYJ (7)) was used to model the three helix-turn-helix WHEP domains $Asp_{749}$-$Pro_{805}$, $Leu_{826}$-$Pro_{878}$, and $Val_{903}$-$Ala_{955}$. Peptide regions ($Pro_{683}$-$Glu_{748}$, $Ala_{806}$-$Ser_{825}$, $Leu_{879}$-$Lys_{902}$, $Thr_{956}$-$Gly_{1015}$) joining the WHEP domains were modeled as unstructured loops.

*IleRS.* A model of full-length human IleRS ($Met_1$-$Phe_{1262}$) was built by homology modeling using multiple crystal structures. The domain $Met_1$-$Ile_{841}$ was modeled based on the crystal structure of IleRS from *Thermus thermophilus* (chain A, PDB ID: 1JZQ (8)), $Ile_{843}$-$Ser_{915}$ was based on LeuRS from *Pyrococcus horikoshii* (chain B, PDB ID: 1WZ2 (9)), $Ile_{918}$-$Ser_{945}$ was based on human pre-mRNA branch site protein p14 (chain B, PDB ID: 2F9D (10)), $Ala_{967}$-$Thr_{1035}$ was based on heterodisulfide reductase from *Methanothermococcus thermolithotrophicus DSM* (chain D, PDB ID: 5ODC (11)), $Ser_{1063}$-$Pro_{1160}$ was based on RANBP/C3HC4-type zinc finger containing protein 1 from *Mus musculus* (chain A, PDB ID: 5Y3T (12)), and $Ser_{1161}$-$Leu_{1256}$ was based on human diubiquitin (chain B, PDB ID: 2Y5B (13)). Homologous crystal structures were not found for $Arg_{946}$-$Asp_{966}$ and $Thr_{1036}$-$Gly_{1062}$, and these regions were modeled *de novo*.

*LeuRS.* A model of near full-length human LeuRS ($Phe_{12}$-$Leu_{1151}$) was built by homology modeling. $Phe_{12}$-$Phe_{1061}$ was modeled based on the crystal structure of LeuRS from *Pyrococcus horikoshii* (chain B, PDB ID: 1WZ2(9)), $Val_{1067}$-$Met_{1116}$ was from ubiquitin-

like protein MDY2 from *Saccharomyces cerevisiae* (chain C, PDB ID: 3ZDM (14)), and $Leu_{1123}$-$Leu_{1151}$ was based on human VPX protein (chain B, PDB ID: 4Z8L). Short missing regions were de novo built with SWISS-MODEL.

*LysRS.* The crystal structure of human LysRS ($Asp_{72}$-$Glu_{576}$) (chain A PDB ID: 6ILD (15)) was used without modification.

*MetRS.* A model of full-length ($Met_1$-$Lys_{900}$) human MetRS was assembled from the crystal structures of the GST-like domain ($Met_1$-$Ala_{211}$) of human MetRS (chain A, PDB ID: 5Y6L (4)), the catalytic domain ($Ala_{226}$-$Ala_{822}$) of human MetRS (PDB ID: 5GL7), and the human MetRS WHEP-TRS domain ($Thr_{835}$-$Lys_{900}$) (PDB ID: 2DJV), plus two *de novo* spacers ($Glu_{212}$-$Leu_{225}$ and $Lys_{823}$-$Val_{834}$). The 14-aa spacer $Glu_{212}$-$Leu_{225}$ that connects the GST-like and catalytic (CD) domains, was modeled as an $\alpha$-helical peptide ($Lys_{729}$-$Lys_{451}$) to position the CD and GST-like domains thus satisfying the constraint of a MetRS-AspRS cross-link. A second 12-aa spacer ($Lys_{823}$-$Val_{834}$) attached the WHEP domain of human MetRS to the CD domain.

*AIMP1.* A model of the human AIMP1 ($Asp_5$-$Lys_{312}$) was assembled from the crystal structure of the N-terminus domain of human AIMP1 ($Asp_5$-$Phe_{80}$) (chain A, PDB ID: 4R3Z(1)), a *de novo*-built $\alpha$-helical structure for $Pro_{81}$-$Lys_{148}$, and a homology model for $Pro_{149}$-$Lys_{312}$ based on the crystal structure of human endothelium monocyte activating polypeptide 2 (EMAPII) (chain A, PDB ID: 1EUJ (16)). AIMP1 conformation was dictated by inter-molecular cross-links with AARSs in the MSC.

*AIMP2.* A model of AIMP2 ($Pro_2$-$Lys_{320}$) was assembled from the crystal structure of N-terminus domain ($Pro_2$-$His_{31}$) of human AIMP2 (chain C, PDB ID: 6ILD(15)), a model of $Glu_{46}$-$Gln_{81}$ based on bifunctional tail protein PIIGCN4 from *Saccharomyces cerevisiae* (PDB ID: 2VNL (17)), and the GST-like domain of human AIMP2 ($Leu_{106}$-$Lys_{320}$) (chain D, PDB ID: 5Y6L (4)). $Gly_{32}$-$Gln_{45}$ and $Thr_{82}$-$Ala_{105}$ domains were *de novo*-built with

SWISS-MODEL. AIMP2 conformation was dictated by cross-links with AARSs in the MSC.

*AIMP3.* The crystal structure of human aminoacyl tRNA synthetase complex-interacting multifunctional protein 3 (AIMP3, $Met_1$-$Asn_{172}$) (chain B, PDB ID: 5Y6L(4)) was used without modification.

**Stepwise assembly of the MSC structural model**

*1. Construction of the pentameric MSC core.* To construct the protein core consisting of monomers of AspRS, MetRS, GluRS, AIMP3, and the GST-like domain of AIMP2, AspRS ($Ala_{21}$-$Asp_{495}$) was first aligned with the AspRS fragment $Pro_{336}$-$Lys_{393}$ from the pentameric crystal structure 5Y6L (chain E) (4). Next, the catalytic domains of MetRS and GluRS were anchored to their corresponding GST-like domains from the crystal structure (chain A and C, PDB ID: 5Y6L (4)) by *de novo*-built spacers (*vide supra*) to satisfy XL-MS-derived intra- and inter-molecular cross-links.

*2. Docking GlnRS.* Before docking GlnRS to the AARS core, the $Arg_{58}$-$Ala_{105}$ domain of AIMP2 was joined to its GST-like domain ($Leu_{106}$-$Lys_{320}$) (chain D, PDB ID: 5Y6L (4)). The human GlnRS model was docked to the AARS core using distance constraints corresponding to GlnRS-GluRS and GlnRS-AIMP2 intermolecular cross-links.

*3. Appending the N-terminus of AspRS.* A *de novo*-built model of the N-terminus domain ($Ala_4$-$Ala_{20}$) of AspRS (*vide supra*) was joined to AspRS and docked to GlnRS using distance constraints corresponding to the peptide bond length between residues $Ala_{20}$ and $Ala_{21}$ of AspRS, and an intermolecular AspRS-GlnRS cross-link.

*4. Docking ArgRS.* ArgRS was docked to the partially assembled MSC using distance constraints corresponding to the intermolecular ArgRS-GlnRS cross-links.

*5. Appending the N-terminus of AIMP1.* We modeled the interaction between the tetramer of GST-like containing proteins and the N-terminus of AIMP1 as reported (18,19). The N-terminus of AIMP1 ($Asp_5$-$Phe_{80}$) (chain A, PDB ID:4R3Z(1)) was docked to the partially assembled MSC so that the N-terminus of the fragment interacts with the GST-like domain of AIMP2, while the C-terminus interacts with AIMP3.

*6. Docking IleRS.* IleRS was docked to the partially assembled MSC in two steps. First, the IleRS model was split into an N-terminus domain ($Met_1$-$Pro_{842}$) and a C-terminus domain ($Ile_{843}$-$Phe_{1262}$), and docked separately to permit conformational flexibility. Initially, the N- and C-terminus domains were positioned such that the peptide bond $Pro_{842}$-$Ile_{843}$ and the intermolecular cross-links of IleRS with MetRS and ArgRS were satisfied. Next, the C-terminus domain ($Ile_{843}$-$Phe_{1262}$) was docked using distance constraints corresponding to the peptide bond length between $Pro_{842}$ and $Ile_{843}$, and the IleRS-ArgRS cross-link. Finally, with the C-terminus domain in place, the N-terminus domain ($Met_1$-$Pro_{842}$) was docked using distance constraints corresponding to the peptide bond between residues $Pro_{842}$ and $Ile_{843}$, and the IleRS-MetRS cross-link.

*7. Appending the C-terminus of LeuRS.* LeuRS was split into N-terminus ($Phe_{12}$-$Phe_{1061}$) and C-terminus ($Arg_{1062}$-$Leu_{1151}$) domains and docked separately. The C-terminus domain was docked first to the partially assembled MSC using distance constraints corresponding to LeuRS-ArgRS and LeuRS-IleRS cross-links.

*8. Docking LysRS.* Monomeric LysRS ($Asp_{72}$-$Glu_{576}$) (chain A, PDB ID: 6ILD (15)) with bound AIMP2 ($Pro_2$-$Glu_{19}$) (chain C, PDB ID: 6ILD (15)) was manually docked to the partially assembled MSC using distance constraints corresponding to the LysRS (chain A)-AIMP2 cross-link. Next, the $Leu_{20}$-$Ser_{57}$ domain of AIMP2 was de novo built and joined to AIMP2. For assembly of the LysRS dimer, chain B was included with chain A as indicated in crystal structure (PDB ID: 6ILD (15)).

*9. Appending the C-terminus of AIMP1.* The C-terminus domain of AIMP1 ($Pro_{81}$-$Lys_{312}$) was threaded through the partially assembled MSC and docked using distance constraints corresponding to the peptide bond between $Phe_{80}$ and $Pro_{81}$ and the AIMP1-ArgRS cross-link. To complete the model of AIMP1, the crystal structure of human EMAPII (chain A, PDB ID: 1EUJ(16)) ($Pro_{149}$-$Lys_{312}$) was joined to AIMP1 and docked using a constraint corresponding to the peptide bond between $Lys_{148}$ and $Pro_{149}$.

*10. Appending the N-terminus of LeuRS.* The N-terminus of LeuRS ($Phe_{12}$-$Phe_{1061}$) was docked satisfying the peptide bond constraint between $Phe_{1061}$ and $Arg_{1062}$.

*11. Appending GluProRS dimer.* The GluProRS dimer was added to the MSC by replacing the GluRS monomer in the assembled MSC with GluRS chain A of the GluProRS dimer.

**REFERENCES – SUPPLEMENTAL DATA**


1. Fu, Y., Kim, Y., Jin, K.S., Kim, H.S., Kim, J.H., Wang, D., Park, M., Jo, C.H., Kwon, N.H., Kim, D. *et al.* (2014) Structure of the ArgRS-GlnRS-AIMP1 complex and its implications for mammalian translation. *Proc. Natl. Acad. Sci. U. S. A.*, **111**, 15084-15089.
2. Kim, K.R., Park, S.H., Kim, H.S., Rhee, K.H., Kim, B.G., Kim, D.G., Park, M.S., Kim, H.J., Kim, S. and Han, B.W. (2013) Crystal structure of human cytosolic aspartyl-tRNA synthetase, a component of multi-tRNA synthetase complex. *Proteins*, **81**, 1840-1846.
3. Ognjenovic, J., Wu, J., Matthies, D., Baxa, U., Subramaniam, S., Ling, J. and Simonovic, M. (2016) The crystal structure of human GlnRS provides basis for the development of neurological disorders. *Nucleic Acids Res.*, **44**, 3420-3431.
4. Cho, H.Y., Lee, H.J., Choi, Y.S., Kim, D.K., Jin, K.S., Kim, S. and Kang, B.S. (2019) Symmetric assembly of a decameric subcomplex in human multi-tRNA synthetase complex via interactions between glutathione transferase-homology domains and aspartyl-tRNA synthetase. *J. Mol. Biol.*, **431**, 4475-4496.
5. Nureki, O., O'Donoghue, P., Watanabe, N., Ohmori, A., Oshikane, H., Araiso, Y., Sheppard, K., Soll, D. and Ishitani, R. (2010) Structure of an archaeal non-discriminating glutamyl-tRNA synthetase: a missing link in the evolution of Gln-tRNAGln formation. *Nucleic Acids Res.*, **38**, 7286-7297.
6. Zhou, H., Sun, L., Yang, X.L. and Schimmel, P. (2013) ATP-directed capture of bioactive herbal-based medicine on human tRNA synthetase. *Nature*, **494**, 121-124.
7. Jeong, E.J., Hwang, G.S., Kim, K.H., Kim, M.J., Kim, S. and Kim, K.S. (2000) Structural analysis of multifunctional peptide motifs in human bifunctional tRNA synthetase: Identification of RNA-binding residues and functional implications for tandem repeats. *Biochemistry*, **39**, 15775-15782.

8. Nakama, T., Nureki, O. and Yokoyama, S. (2001) Structural basis for the recognition of isoleucyl-adenylate and an antibiotic, mupirocin, by isoleucyl-tRNA synthetase. *J. Biol. Chem.*, **276**, 47387-47393.
9. Fukunaga, R., Ishitani, R., Nureki, O. and Yokoyama, S. (2005) Crystallization of leucyl-tRNA synthetase complexed with tRNALeu from the archaeon Pyrococcus horikoshii. *Acta Crystallogr .Sect. F Struct. Biol. Cryst. Commun.*, **61**, 30-32.
10. Schellenberg, M.J., Edwards, R.A., Ritchie, D.B., Kent, O.A., Golas, M.M., Stark, H., Luhrmann, R., Glover, J.N. and MacMillan, A.M. (2006) Crystal structure of a core spliceosomal protein interface. *Proc. Natl. Acad. Sci. U. S. A.*, **103**, 1266-1271.
11. Wagner, T., Koch, J., Ermler, U. and Shima, S. (2017) Methanogenic heterodisulfide reductase (HdrABC-MvhAGD) uses two noncubane [4Fe-4S] clusters for reduction. *Science*, **357**, 699-703.
12. Fujita, H., Tokunaga, A., Shimizu, S., Whiting, A.L., Aguilar-Alonso, F., Takagi, K., Walinda, E., Sasaki, Y., Shimokawa, T., Mizushima, T. *et al.* (2018) Cooperative domain formation by Hhomologous motifs in HOIL-1L and SHARPIN plays a crucial role in LUBAC stabilization. *Cell Rep.*, **23**, 1192-1204.
13. Ye, Y., Akutsu, M., Reyes-Turcu, F., Enchev, R.I., Wilkinson, K.D. and Komander, D. (2011) Polyubiquitin binding and cross-reactivity in the USP domain deubiquitinase USP21. *EMBO Rep.*, **12**, 350-357.
14. Tung, J.Y., Li, Y.C., Lin, T.W. and Hsiao, C.D. (2013) Structure of the Sgt2 dimerization domain complexed with the Get5 UBL domain involved in the targeting of tail-anchored membrane proteins to the endoplasmic reticulum. *Acta Crystallogr. D. Biol. Crystallogr.*, **69**, 2081-2090.
15. Hei, Z., Wu, S., Liu, Z., Wang, J. and Fang, P. (2019) Retractile lysyl-tRNA synthetase-AIMP2 assembly in the human multi-aminoacyl-tRNA synthetase complex. *J. Biol. Chem.*, **294**, 4775-4783.

16. Kim, Y., Shin, J., Li, R., Cheong, C., Kim, K. and Kim, S. (2000) A novel anti-tumor cytokine contains an RNA binding motif present in aminoacyl-tRNA synthetases. *J. Biol. Chem.*, **275**, 27062-27068.
17. Seul, A., Muller, J.J., Andres, D., Stettner, E., Heinemann, U. and Seckler, R. (2014) Bacteriophage P22 tailspike: structure of the complete protein and function of the interdomain linker. *Acta Crystallogr. D. Biol. Crystallogr.*, **70**, 1336-1345.
18. Schwarz, M.A., Lee, D.D. and Bartlett, S. (2018) Aminoacyl tRNA synthetase complex interacting multifunctional protein 1 simultaneously binds Glutamyl-Prolyl-tRNA synthetase and scaffold protein aminoacyl tRNA synthetase complex interacting multifunctional protein 3 of the multi-tRNA synthetase complex. *Int. J. Biochem. Cell Biol.*, **99**, 197-202.
19. Norcum, M.T. and Warrington, J.A. (2000) The cytokine portion of p43 occupies a central position within the eukaryotic multisynthetase complex. *J. Biol. Chem.*, **275**, 17921-17924.